Biomimetic monolayer films of digalactosyldiacylglycerol incorporating plastoquinone

Javier Hoyo[1,2], Ester Guaus[1], Juan Torrent-Burgués[1,2,], Fausto Sanz[2,3]*

[1]Universitat Politècnica de Catalunya, Dpt. Chemical Engineering, 08222 Terrassa (Barcelona), Spain

[2]Institut de Bioenginyeria de Catalunya (IBEC), 08028 Barcelona, Spain

[3]Universitat de Barcelona, Dpt. Physical-Chemistry, 08028 Barcelona, Spain.

*Corresponding autor: juan.torrent@upc.edu, C/ Colom 1, E-08222 Terrassa (Barcelona), Spain, Tlf: +34 937398043.

Abstract

The photosynthesis is the process used by plants and bacteria cells to convert inorganic matter in organic thanks to the light energy. This process consist on several steps, being one of them the electronic transport from the photosystem II to the cytochrome thanks to plastoquinone-9 (PQ). Here we prepare membranes that mimic the characteristics and composition of natural photosynthetic cell membranes and we characterize them in order to obtain the PQ molecules position in the membrane and their electrochemical behaviour. The selected galactolipid is digalactosyldiacylglycerol (DGDG) that represents the 30% of the thylakoid membrane lipid content. The results obtained are worthful for several science fields due to the relevance of galactolipids as anti-algal, anti-viral, anti-tumor and anti-inflamatory agents and the antioxidant and free radical scavenger properties of prenylquinones.

Both pure components (DGDG and PQ) and the DGDG:PQ mixtures have been studied using surface pressure-area isotherms. These isotherms give information about the film stability and indicates the thermodynamic behaviour of the mixture and their physical state. The Langmuir-Blodgett (LB) film has been transferred forming a monolayer that mimics the bottom layer of the biological membranes. This monolayer on mica has been topographically characterized using AFM and both the height and the physical state that they present have been obtained. Moreover, these monolayers have been transferred onto ITO that is a hydrophilic substrate with good optical and electrical features, so that, it is suitable for studying the electrochemical behaviour of these systems and it is a good candidate for energy producing devices.

Keywords

Biomimetic membrane, digalactosyldiacylglycerol, plastoquinone, modified ITO electrode, Langmuir-Blodgett film, electron transfer.

Abbreviations

AFM	Atomic Force Microscopy
ATP	Adenosine triphosphate
CV	Cyclic voltammogram
DGDG	Digalactosyldiacylglycerol
HPT	Head plus part of the tail
ITO	Indium-tin oxide
LB	Langmuir-Blodgett
LC	Liquid Condensed state
LE	Liquid Expanded state
LPT	Last part of the tail
MGDG	Monogalactosyldiacylglycerol
PQ	Plastoquinone
S	Solid state
UQ	Ubiquinone

Highlights

Biomimetic films of digalactosyldiacylglycerol inserting plastoquinone have been built

Plastoquinone presents two main positions in the lipid matrix: diving and swimming

The different plastoquinone positions lead to different redox processes

Plastoquinone (PQ) positions are tuned by the surface pressure and PQ initial content

1. Introduction

Artificial lipid bilayers have been extensively studied as membrane models that mimic natural membranes, so they are also called biomimetic membranes. They have shown their relevance in a broad range of chemical and biological applications, being one of the most encouraging the development of artificial photoelectric devices [1-5]. The thylakoid membrane of chloroplasts of oxygenic organisms is the site where the photochemical and electron transport reactions of photosynthesis take place. In particular, the electron and proton shuttle between photosystem II and cytochrome is carried by platoquinone-9 (PQ) (Figure 1A) in higher plants. On the other hand, the thylakoid membrane is constituted by a lipid matrix that avoids the free diffusion of ions, maintains the fluidity of the membrane and allows an electrochemical potential difference across this membrane, which is required for the ATP synthase [6]. The 70% of the thylakoid membrane area is occupied by proteins and the rest is mainly constituted by lipids. This thylakoid membrane harbours the protein complexes of the oxygenic photosynthetic machinery [7]. On the other hand, the lipidic content of the thylakoid matrix depends on the specie and the external conditions. However, it can be agreed that the thylakoid membrane of a typical higher plant is composed by the following lipids: monogalactosyldiacylglycerol (MGDG) ≈ 50% (Figure 1C), digalactosyldiacylglycerol (DGDG) ≈ 30% (Figure 1D), sulfoquinovosyldiacylglycerol ≈ 5-10%, phosphatidylglycerol ≈ 5-10% [7] and small amounts of other lipids [8,9].

In order to prepare reliable membranes that can mimic the natural photosynthesis, the lipidic content and the chemical nature of this membrane should be close to the natural ones. Moreover, it is also of great relevance the position knowledge of the redox molecules in the biomimetic matrix due to it affects the electron transfer process. The position of the ubiquinone-10 (UQ) (Figure 1B), which is similar in size and shape to PQ, has been studied in several attempts on phospholipid bilayers that light different conclusions. However, there is consensus about that UQ has two main positions in a lipid bilayer [10], which are called by Söderhäl and Laaksonen [11] as “diving quinone” and “swimming quinone”. “Diving quinone” is characterized by an inflexion point in the hydrocarbon tail of the UQ, which separates the UQ molecules in the head plus part of the tail (HPT) and the last part of the tail (LPT). HPT is placed in parallel to the lipid chains, inserted between them, whereas LPT is free to move. LPT can adopt two configurations, first, perpendicular to the lipid chains, and second, inserted in parallel between the lipid chains of the opposite leaflet where the HPT is.

This second position of LPT, although it may seem unfavoured, is stable due to the similar properties between the UQ tail and the lipid chains, and so that, it is soluble in this region [11]. Söderhäl and Laaksonen [11] simulations suggest that the UQ headgroup, in the lamellar state of the SPB, is placed between the 3rd and the 6th carbon atom of the lipid chain counted from the carbonyl carbon, which is consistent with the previous studies of Aranda et al. [12].

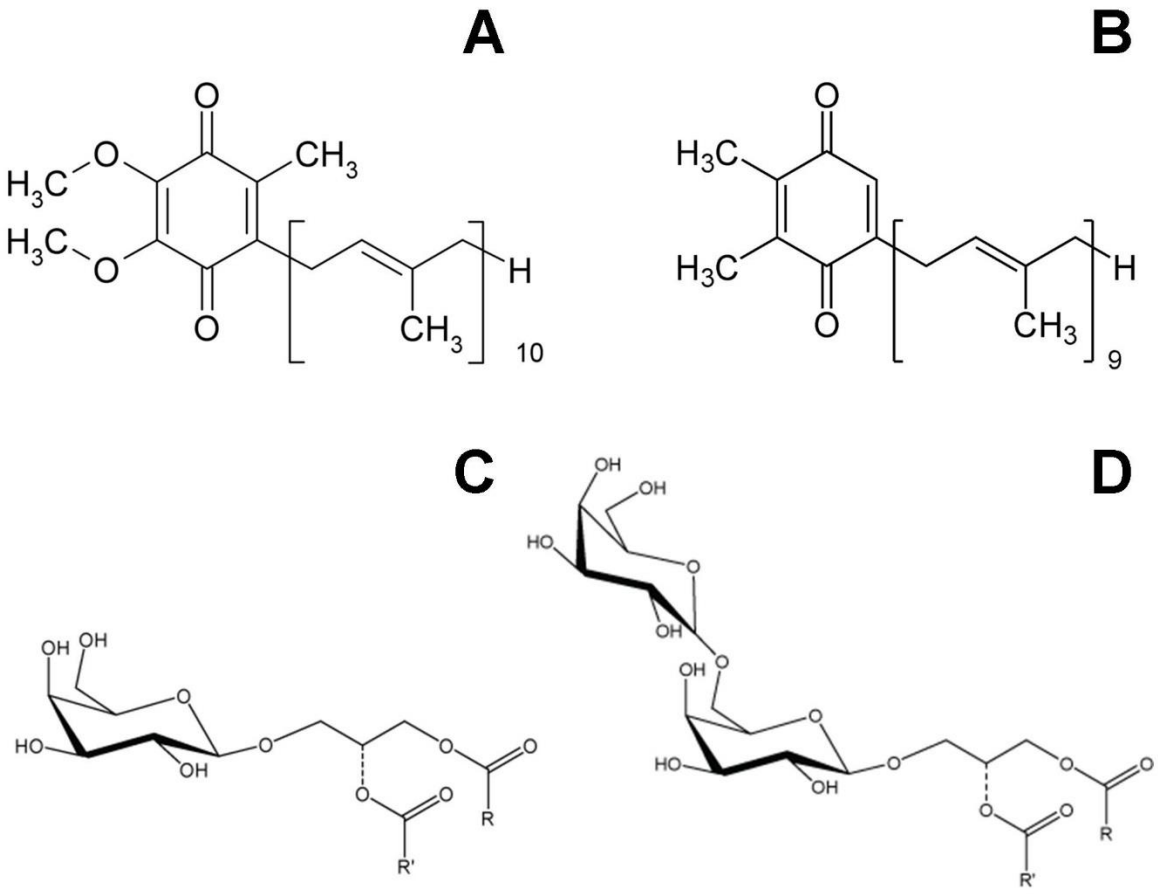

Figure 1. Scheme of a molecule of (A) UQ-10, (B) PQ-9, (C) MGDG and (D) DGDG.

The "swimming" position is characterized by the flexible hydrocarbon tail of UQ, which moves randomly on the midplane and the corresponding UQ head can move a maximum of ≈ 1 nm in the lipid chains of both sides of the bilayer [11]. The "swimming" position is more stable than the "diving" position due to, in the later, the cooperative motions between the lipid chains are disrupted by the intrusion of the UQ head. Moreover, the midplane is less molecule crowded and it has lower viscosity ($2 \cdot 10^{-3}$ Pa·s) than the polar head region (0.1-0.2 Pa·s), so being favoured the UQ position in this midplane [13,14]. The position corresponding to

"diving quinone" has been proposed using several techniques [12, 15-18], and similar occurs with the "swimming" position [10,19-21].

In this work we use the Langmuir and Langmuir-Blodgett (LB) techniques to prepare biomimetic monolayers of the DGDG:PQ systems due to the high control over the membrane structure that the LB technique confers compared with other techniques for biomimetic membranes formation that include vesicle fusion [22]. These monolayers are studied using surface pressure – Area, π-A, isotherms and their data are processed to light their physical states and mixing behaviour. These monolayers, once transferred to a solid substrate at several surface pressures (including the natural membranes internal lateral surface pressure ≈ 33 $mN \cdot m^{-1}$ [23]) will be topographically studied using Atomic Force Microscopy (AFM) to observe the influence of PQ in the DGDG matrix. Finally, we use the cyclic voltammetric technique for studying the electrochemical behaviour of the monolayers once transferred to indium-tin oxide (ITO), which has good optical and electrical properties, so converting ITO in the perfect candidate for studying artificial photosynthesis and other energy producing devices [24]. Moreover, the results obtained are worthful for several science fields due to the relevance of galactolipids as anti-algal, anti-viral, anti-tumor and anti-inflamatory agents and the antioxidant and free radical scavenger properties of prenylquinones [25].

2. Materials and methods

2.1 Materials

PQ was provided by ASM Research Chemicals and DGDG, with acyl = stearoyl (18:0), was purchased from Matreya (USA). KH_2PO_4, KCl and chloroform of analytical grade from Sigma-Aldrich were used in solutions preparation. Water was ultrapure MilliQ® (18.2 MΩ·cm). Mica sheets were purchased from TED PELLA Inc (CA) and ITO deposited on glass slides were purchased to SOLEMS (France).

2.2 Methods

2.2.1 Monolayer formation

Langmuir and Langmuir-Blodgett monolayer formation were carried on a trough (Nima Technology, Cambridge, UK) model 1232D1D2 equipped with two movable barriers. The surface pressure was measured using paper Whatman 1 held by a Wilhelmy balance connected to a microelectronic system registering the surface pressure (π). The subphase used in these experiments was MilliQ® quality water. Previous to the subphase addition, the trough was cleaned twice with chloroform and once with MilliQ® quality water. Residual impurities were cleaned from the air|liquid interface by surface suctioning. The good baseline in the π–A isotherms confirms the interface cleanliness. Solutions of DGDG, PQ and DGDG:PQ were prepared using chloroform and spread at the air|liquid interface using a high precision Hamilton microsyringe. Barrier closing rates were fixed at 50 $cm^2 \cdot min^{-1}$ (8.4 $Å^2 \cdot molec^{-1} \cdot min^{-1}$) for isotherm registration and at 25 $cm^2 \cdot min^{-1}$ (4.2 $Å^2 \cdot molec^{-1} \cdot min^{-1}$) for LB film transfer. No noticeable influence of these compression rates was observed on the isotherm shape. Isotherm recording was carried out adding the solution to the subphase and waiting 15 minutes for perfect spreading and solvent evaporation. Experiments were conducted at 21±1ºC and repeated a minimum of three times for reproducibility control.

LB monolayers were transferred to mica surface for AFM characterization and to ITO for electrochemical characterization, at defined surface pressure values. Mica surface has lower roughness than ITO surface at a nanometric scale, which permits the best observation of the monolayer films. LB film transfer was conducted dipping the substrate, freshly cleaved mica or cleaned ITO, through the air|liquid interface on the subphase before adding the solution, and five minutes were lagged after pressure setpoint was achieved. Transfer speed was set at 5 $mm \cdot min^{-1}$ linear velocity. The transfer ratios obtained for mica are close to 100% at each surface pressure, and those for ITO are similar except for the lower surface pressure of 3 $mN \cdot m^{-1}$ where the transfer ratio is close to 80%.

2.2.2 AFM characterization

The AFM topographic images of LB films were acquired in air tapping mode using a Multimode AFM controlled by Nanoscope IV electronics (Veeco, Santa Barbara, CA) under ambient conditions. Triangular AFM probes with silicon nitride cantilevers and silicon tips were used (SNL-10, Bruker) which have a nominal spring constant ≈ 0.35 $N \cdot m^{-1}$ and a

resonant frequency of 50 kHz. Images were acquired at 1.5 Hz line frequency and at minimum vertical force to reduce sample damage. AFM images were obtained from at least two different samples, prepared on different days, and by scanning several macroscopically separated areas on each sample.

2.2.3 Electrochemical characterization

The voltammetric measurements were performed in a conventional three-electrode cell using an Autolab Potentiostat-Galvanostat PGSTAT-12 (Ecochemie, NL). Working electrodes were freshly-cleaned ITO slides (10 mm x 25 mm) cleaned once with ethanol and three times with MilliQ® grade water. Counter electrode was a platinum wire in spiral geometry and the reference electrode was an Ag/AgCl/3M KCl microelectrode (DRIREF-2SH, World Precision Instruments). This reference electrode was mounted in a Lugging capillary containing KCl solution at the same cell concentration. All reported potentials were referred to this electrode. The electrochemical cell contained 0.150 M KCl as supporting electrolyte at pH 7.4 adjusted with the KH_2PO_4/K_2HPO_4 buffer solution. This pH is in the range of physiological pH of cells. All solutions were freshly prepared with MilliQ® grade water de-aerated with a flow of Ar gas for 15 min prior to the cyclic voltammetry (CV) experiments, which were conducted at 22 ± 1ºC. Voltammetric experiments were carried out at several scan rates, scanning towards cathodic potentials in a homemade glass cell with a reaction area of 33 mm^2.

3 Results and Discussion

3.1 π-A isotherms, physical states and mixing behaviour

The π-A isotherms of DGDG, PQ and their mixtures at biological relevant ratios referred to the DGDG area per molecule are presented in Figure 2. Inset of Figure 2 represents the C_s^{-1} curves corresponding to the described π-A isotherms, and they are calculated according to the Equation 1.

$$C_s^{-1} = -A\left(\frac{d\pi}{dA}\right)_T \quad (1)$$

The most significant values of Figure 2 are summarized in Table I.

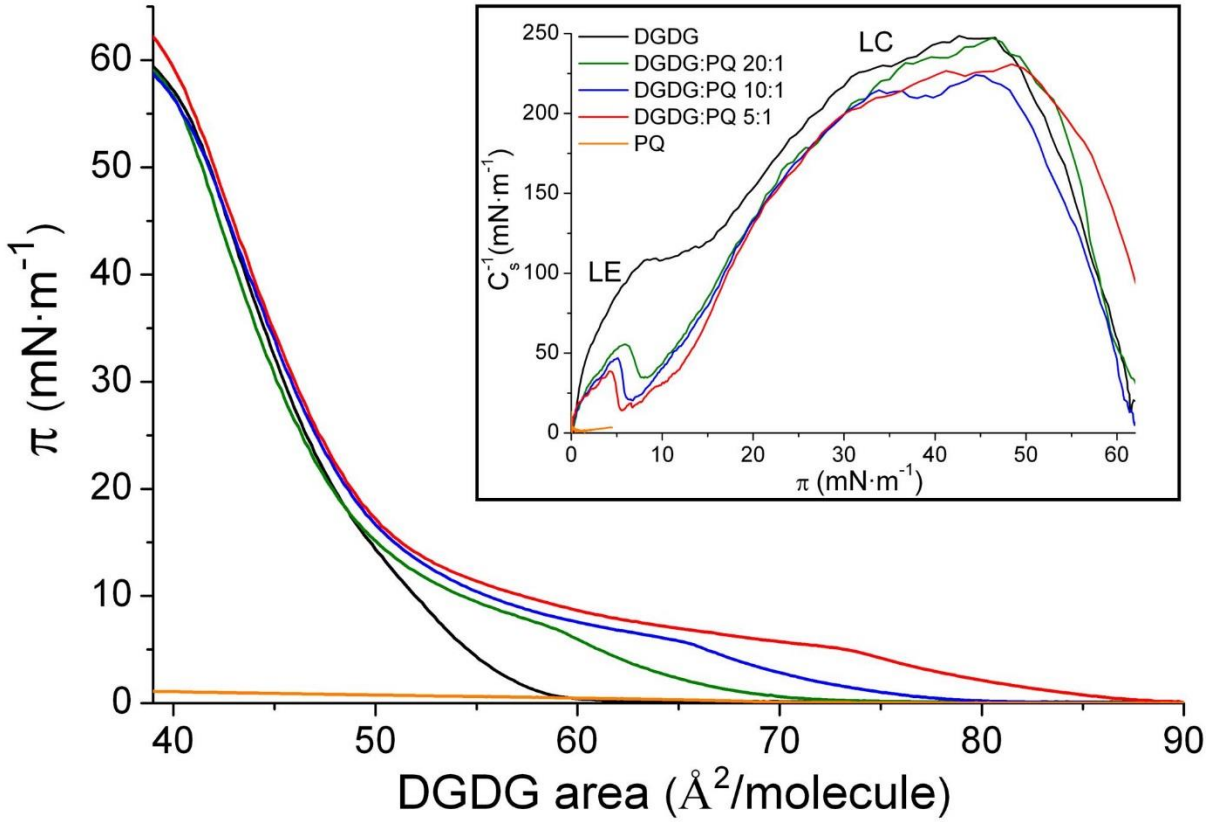

Figure 2. π-A isotherms for DGDG, PQ and DGDG:PQ mixtures at 21 ± 1 ºC on water subphase. Inset: Inverse of the compressibility modulus vs. surface pressure for DGDG, PQ and DGDG:PQ mixtures on water subphase.

The isotherms show that DGDG and DGDG:PQ systems form stable monolayers. DGDG:PQ mixtures present different initial zone ($\pi \leq 15$ mN·m^{-1}) behaviour according to the PQ presence in the mixture. At $\pi > 15$ mN·m^{-1}, all π-A isotherms of the mixtures resemble the pure DGDG indicating that the PQ has been mostly expelled from the DGDG matrix. So that, the remaining PQ molecules have been accommodated producing little effect on the headgroups packing.

Table I. Collapse pressure, lift-off area and kink point position for the DGDG, PQ and their biological mixtures obtained from Figure 2.

	Collapse pressure (mN·m^{-1})	Lift-off area (Å^2·molec^{-1})	Kink point pressure (mN·m^{-1})	Kink point area (Å^2·molec^{-1})
DGDG	57	59	-	-
DGDG:PQ 20:1	58	72	5.7	60.3
DGDG:PQ 10:1	58	77	5.1	66.3
DGDG:PQ 5:1	60	86	4.3	74.9
PQ	0.3	76	-	-

Both the lift-off area and the area at which appears the kink point (local minimum point in the C_s^{-1} curve that represents changes from concave to convex or vice-versa in the π-A isotherms) increase as the PQ content in the DGDG:PQ mixture is enlarged (Table I) and it is correlated with the distorting effect of PQ in the DGDG matrix [26]. This phenomena was also observed by Kruk et al. [27] using PQ and unsaturated MGDG and also by Bilewicz et al. [28] using UQ and $C_{18}SH/C_{18}OH$. The presence of PQ in the initial zone hindrances the packing of the DGDG headgroups, and therefore, the hydrophobic interactions between the DGDG chains are also reduced, as it was seen in the case of UQ inserted in phospholipids [26,29]. The explanation for this phenomenon is that PQ is better retained in the lipid monolayer when present at low concentrations due to it affects in a lower extent the formation and shape of the ordered phases.

All the C_s^{-1} curves for the DGDG:PQ mixtures present a similar behaviour showing the kink point at $\pi \approx 5$ mN·m^{-1}. This kink point, accordingly to the values presented by Vitovic et al. [30] and the characteristics of this system, indicates the phase change from liquid expanded (LE) to liquid condensed (LC) and it implies the main PQ expulsion from the lipid matrix. The extent of this rejection and the surface pressure at which takes place depends on the initial PQ content. At $\pi > 15$ mN·m^{-1} the mixtures and the pure DGDG present a similar C_s^{-1} curves shape (Inset of Figure 2), which is correlated with a similar PQ content remaining between the lipid chains. However, the mixtures present slightly lower C_s^{-1} values than the pure DGDG, which corroborate that the presence of the remaining PQ slightly hindrances the perfect packing of the mixtures.

Phase rule

The collapse pressure of a mixed monolayer of different components is related to the miscibility of its components, being dependent on the film composition in a miscible system [31,32]. In our DGDG and DGDG:PQ mixtures isotherms, the collapse pressure is ≈ 58 mN·m^{-1}. Therefore, the similar collapse pressure can be used to elucidate the expulsion of one of the components in a mixed film. In a two component monolayer, if components are completely immiscible, a lower collapse pressure of one of the components will be observed as predicted by the phase rule. Maintaining temperature and external pressure constant, the

number of degrees of freedom F of the monolayer system is given by the Equation 2 [33,34], where C_B is the number of components in the bulk, C_S is the number of components confined to the surface, P_B is the number of bulk phases, and P_S is the number of monolayer phases in equilibrium with each other.

$$F = C_B + C_S - P_B - P_S + 1 \quad (2)$$

In our DGDG:PQ experiments, at the air|water interface, C_B = 2 (air and water), C_S = 2 (DGDG and PQ), and P_B = 2 (gas and liquid), thus $F = 3 - P_S$. According to that, homogenous mixed films achieve the collapse equilibrium with P_S = 2 (condensed and collapsed state), so the system will have one degree of freedom. According to our results, the collapse pressure is practically fixed, discarding the experimental deviations, for pure DGDG and DGDG:PQ mixtures. This indicates zero degrees of freedom and therefore, following the previous reasoning, P_S = 3. So that, at the collapse equilibrium of the mixtures isotherms coexist DGDG (LC), DGDG (collapse) and expelled PQ. The same statements can also be applied to the phase change zone at $\pi \approx 5$ mN·m^{-1}, where π is practically fixed indicating zero degrees of freedom. Thus P_S = 3, which indicate that three phases coexist: DGDG:PQ (LE), DGDG:PQ (LC) and expelled PQ, confirming the beginning of the PQ expulsion at this surface pressure. This observation coincides with the AFM conclusions.

Thermodynamic study

The representation of the mean area per molecule vs. the molar fraction at selected pressures gives idea about the ideality of a mixture at these surface pressures (Equation 3). On the other hand, the representation of the ΔG_{mix} vs. PQ molar fraction gives idea about the stability of the mixture (Equations 4-6).

$$A^E = A_{12} - (x_1 A_1 + x_2 A_2) \quad (3)$$

$$G^E = N_A \int_0^{\pi} A^E d\pi \quad (4)$$

$$\Delta G_{mix} = \Delta G_{id} + G^E \quad (5)$$

$$\Delta G_{id} = RT(X_1 \ln X_1 + X_2 \ln X_2) \quad (6)$$

Where A^E is the excess area, A_{12} the mean area per molecule for the mixture. A_1 and A_2 the area per molecule for the individual components and x_1 and x_2 the molar fraction of each component. G^E is the excess free energy of mixing and ΔG_{mix} the free energy of mixing. On

the other hand, N_A is the Avogadro's number, R the gas constant and T the absolute temperature.

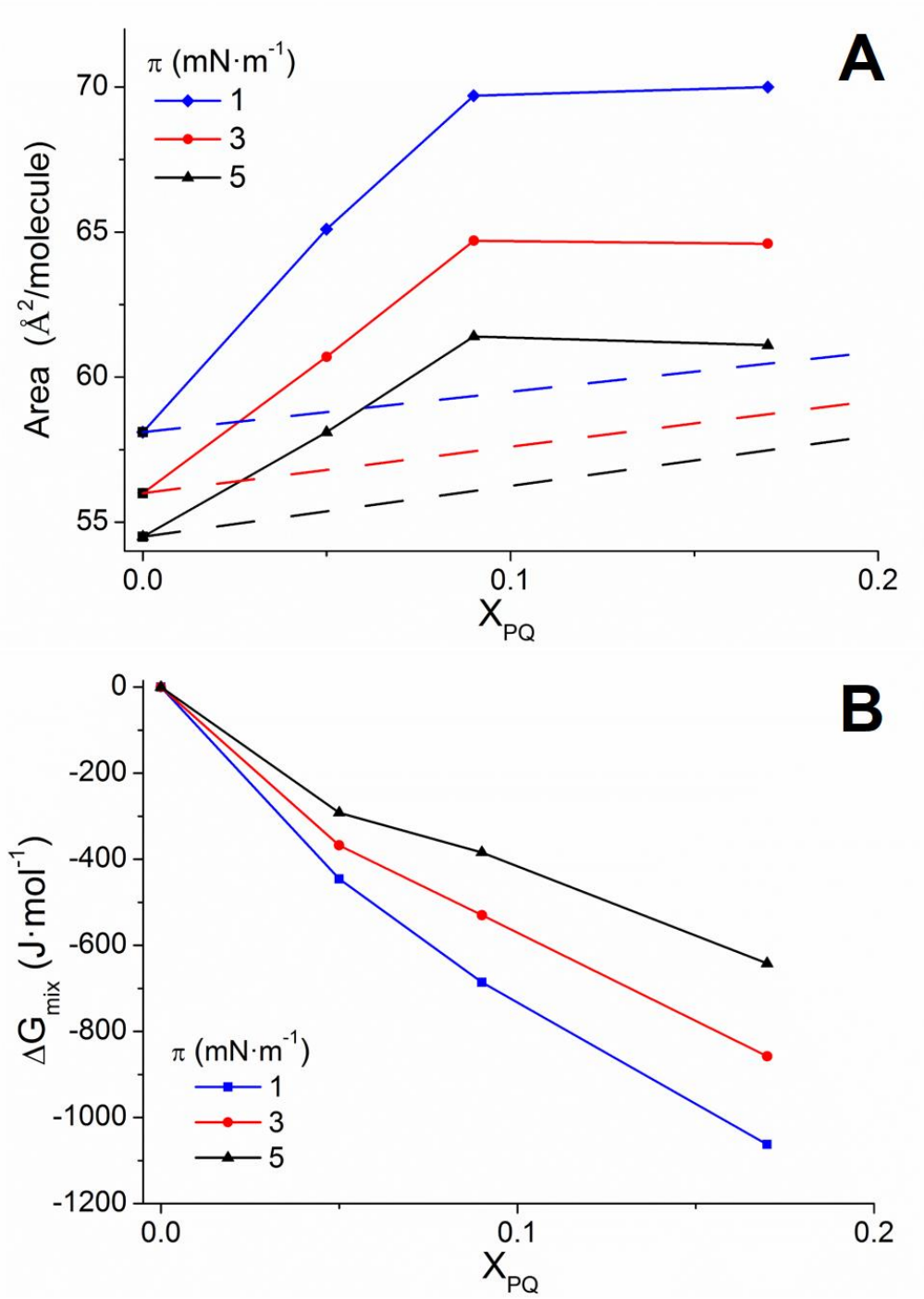

Figure 3. A) Plot of the mean area per molecule vs. the molar fraction for DGDG, PQ and DGDG:PQ mixtures at several surface pressures before the main PQ expulsion. Discontinuous straight line represents the ideal behaviour for each surface pressure. B) Plot of the mixing energy vs. the molar fraction for DGDG, PQ and DGDG:PQ mixtures at several surface pressures before the main PQ expulsion.

The Figure 3A plots the area per molecule vs. the PQ molar fraction, represented for DGDG:PQ mixtures at several surface pressures before the main PQ expulsion (≈ 5 $mN \cdot m^{-1}$). At surface pressures above this event, the thermodynamic study has not been performed due to the PQ content in the DGDG:PQ matrix is unknown and significantly lower than the initial presence. Figure 3A show that DGDG and PQ form non-ideal mixtures with positive deviation at $\pi \leq 5$ $mN \cdot m^{-1}$, which indicates that, at these surface pressures, the interactions between the two components are weaker than the interactions between pure components [35] suggesting the possible formation of enriched domains or aggregates of molecules [32,34] at high PQ content. The Figure 3B represents the ΔG_{mix} vs. PQ molar content at several surface pressures before the main PQ expulsion. The negative values observed for ΔG_{mix} at $\pi \leq 5$ $mN \cdot m^{-1}$ indicate that the mixed monolayers of DGDG:PQ are more stable than pure components [35], although the low ΔG_{mix} values corroborate the low stability of the mixture. The formation of non-ideal mixtures between PQ and DGDG at low surface pressure is explained by the difference in the chain length between PQ and DGDG, which permits a free rotation of the PQ part that protrudes over the DGDG, producing also a motion of the DGDG molecules that induces an increase of the molecular area [35,36].

3.2 AFM

We present the topographic images of DGDG and several DGDG:PQ mixtures at several surface pressures to light which the organization of these molecules is once transferred to a hydrophilic substrate (mica) and ultimately, correlate this knowledge with the predicted results in previous sections. Figure 4 presents the AFM topographic images corresponding to DGDG transferred at several surface pressures on mica. The images present two tonalities of brown (fair and dark) and the height measurements indicate that both correspond to zones with different heights of the DGDG monolayer. The measurements of the relative height of the higher fair zones referred to the dark zones in Figure 4 is 15 ± 1 Å. This information indicates that the monolayer, once transferred to the mica surface, presents zones with a different tilting of the DGDG molecules that indicate a different physical state. It is important to remark that each brown tonality indicates a different height but the physical state that is correlated with them depends on the surface pressure at which the monolayer has been transferred.

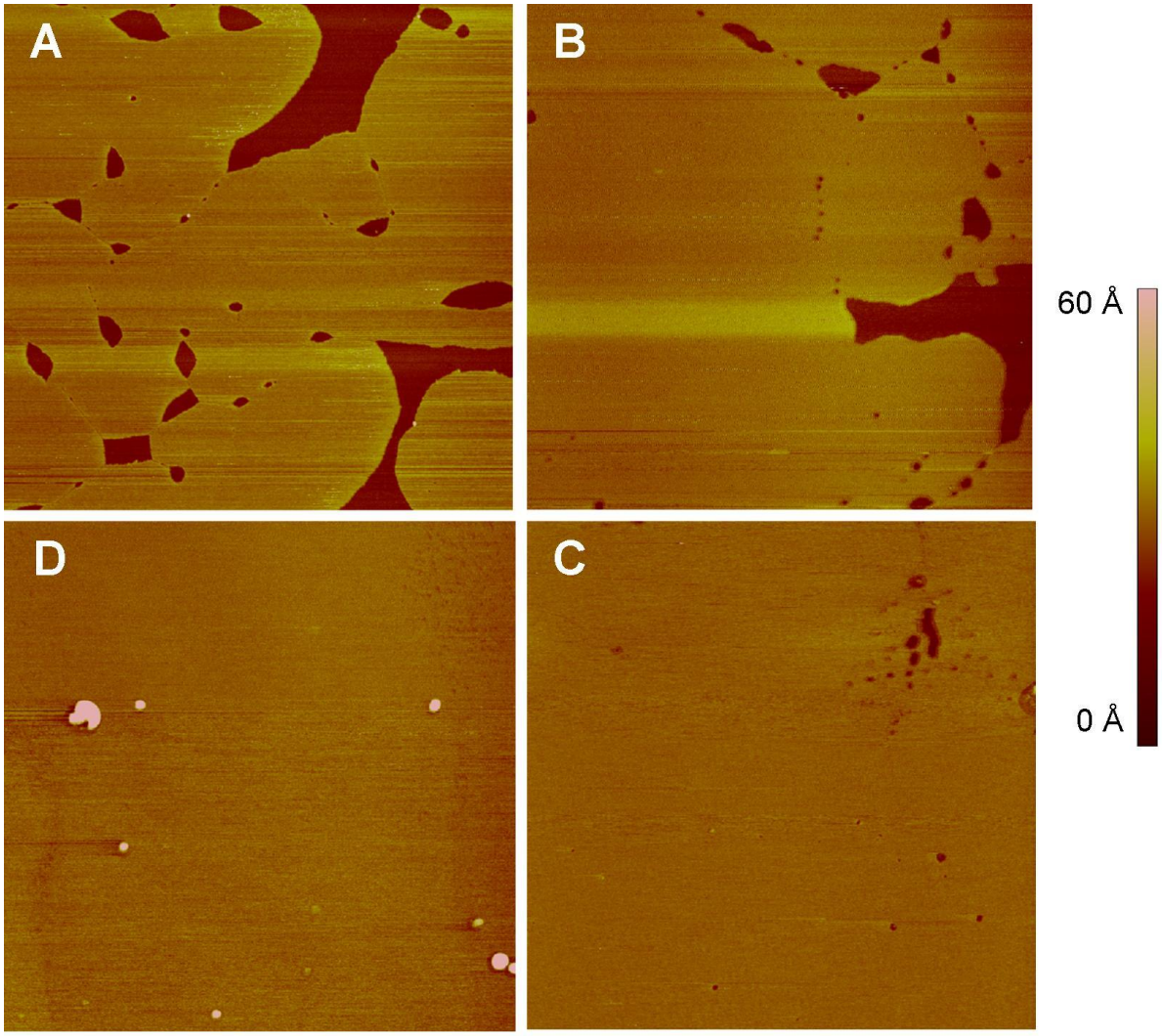

Figure 4. AFM images (5µm x 5µm) for LB films of DGDG transferred on mica at 21ºC at (A) $\pi = 3$ mN·m^{-1}, (B) $\pi = 15$ mN·m^{-1}, (C) $\pi = 33$ mN·m^{-1}, (D) $\pi = 45$ mN·m^{-1}.

DGDG on mica at low surface pressures ($\pi \leq 3$ mN·m^{-1}) forms round edge domains of a compact state (Image A) whereas the rest of the molecules are in a more fluid state. The compression of the film leads to the ordering of the fluid phase (Images B and C in Figure 4) till the ordered state covers the entire mica surface (Figure 4D). At $\pi = 45$ mN·m^{-1} this compact monolayer surface presents some rounded shape structures, which origin is uncertain but we hypothesize that they are the result of a local surface pressure increase that induces a local collapse [37,38] of the film, forming flatten disks of ≈100 - 200 nm diameter and a height of 3 to 20 nm. These observations are consistent with small flatten bilayer vesicles, in line with previous observations for POPG [39] and DPPG [40].

The relative height of the more ordered phase respectively to the less ordered phase has been measured in order to clarify which physical state predominates at each surface pressure. The $C_{s\ \max}^{-1}$ values presented in the inset Figure 2 indicate that S state is never achieved by DGDG, so in Figure 4A, we correlate the relative height of 15 ± 1 Å to the LC1 state referred to the LE state (dark zones), corresponding the molecules in LC1 to the molecules at the beginning of the LC state (medium brown). The relative height of 3 ± 1 Å observed in Figure 4C is correlated with the LC2 state, molecules at the more ordered state of the LC state (fair zones), referred to LC1 (dark zones). Therefore, fair zones at π = 3 mN·m^{-1} corresponds to the LC1 state and at higher surface pressure, they represent the LC2 state. On the other hand, dark zones corresponds to the LE state at π = 3 mN·m^{-1} that changes to LC at higher surface pressures. The compression of the less ordered state transforms gradually the LC1 zones on LC2, remaining small LC1 areas that achieve rounded shape when the surface pressure is increased (Figure 4C). These topographic results for saturated DGDG differs to the observations of Bottier at al. [41] and Chu et al. [42] who observed homogeneous LE phase images with no visible phase separation for unsaturated DGDG at several surface pressures.

The height of the LE phase of galactolipid-prenylquinone systems has been estimated in 6 ± 2 Å based on the height observed for the LE state of the MGDG:UQ system [26]. Moreover, this LE height is in accordance to the 3-6 Å observed in the literature for LE of DPPC [43,44]. Accepting that this value should be close to that of the DGDG, we calculate the absolute height of each physical state according to it and the relative heights previously measured (Table II).

Table II. Height (in Å) of each physical state for the LB monolayers of DGDG and DGDG:PQ mixtures on mica. *Estimated value (more information in the text).

	LE	LC1	LC2
DGDG	6 ± 2 *	21 ± 2	24 ± 2
DGDG:PQ 20:1	6 ± 2 *	22 ± 2	24 ± 2
DGDG:PQ 10:1	6 ± 2 *	19 ± 2	25 ± 2
DGDG:PQ 5:1	6 ± 2 *	21 ± 2	23 ± 2

Figure 5 shows the AFM topographic images corresponding to pure DGDG and the selected DGDG:PQ mixtures transferred on mica at π = 3 mN·m^{-1}. The surface pressure used permits

us to ensure that PQ is present in all the mixtures showing the larger differences for these systems. The images A-D show two different tonalities of brown (fair and dark) and both correspond to the DGDG or DGDG:PQ monolayer, being each tonality correlated with a different physical state of the system monolayer. On the other hand, the images A-D show that the PQ content has non-influence on the ordered domains size whereas it affects to the area occupied by these domains, being increased when lowering the initial PQ content.

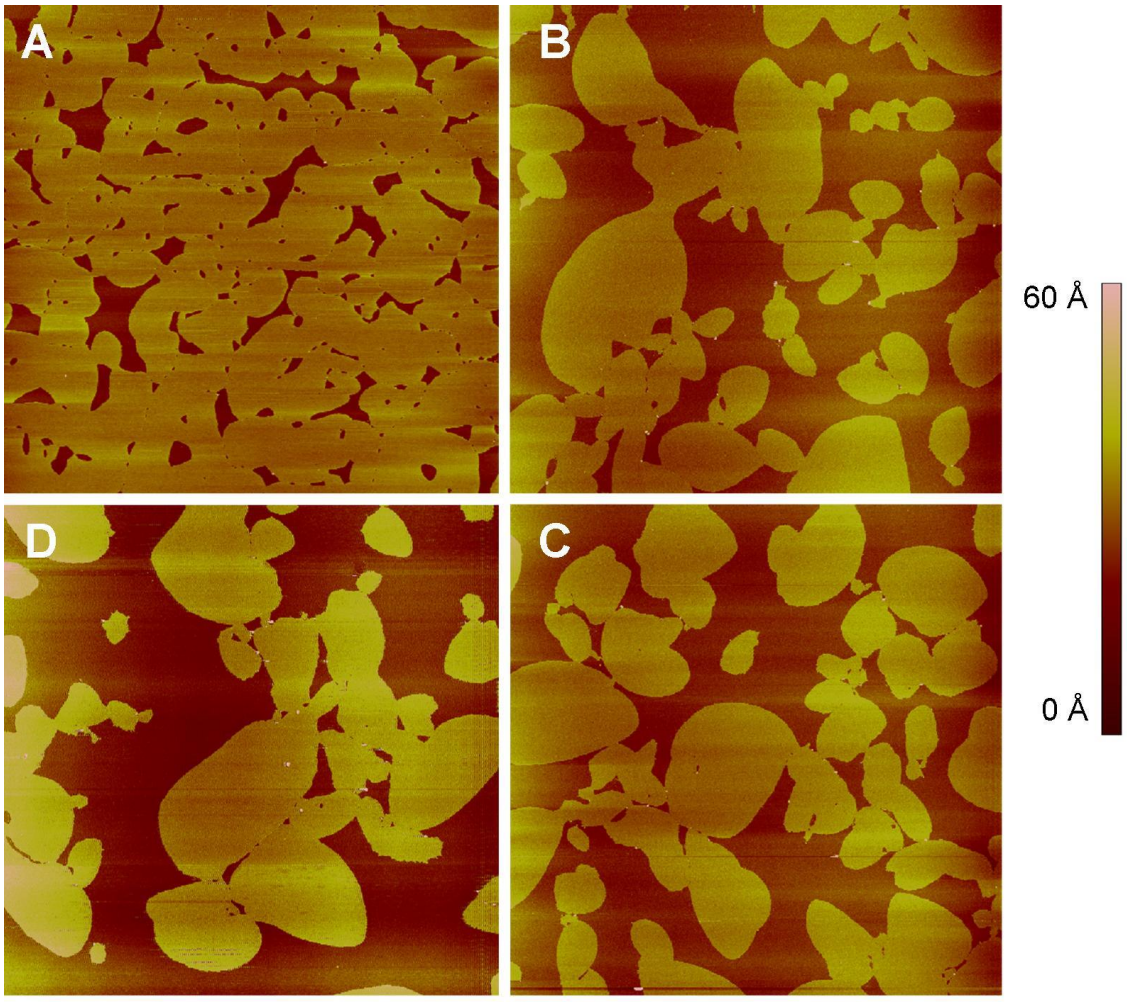

Figure 5. AFM images (20µm x 20µm) for LB films transferred on mica at 21ºC at π = 3 mN·m^{-1} for (A) pure DGDG and DGDG:PQ systems (B) 20:1, (C) 10:1, (D) 5:1.

In order to explain the behaviour of the DGDG:PQ mixtures at several surface pressures, we have selected the 5:1 ratio (Figure 6) due to it is the most different from the pure DGDG (Figure 4) of the ratios we have studied and it represents the best option to compare them. The results obtained for the DGDG:PQ system, as it has been seen for pure DGDG, indicate that each brown tonality indicates a different height but the physical state that is correlated with

them depends on the surface pressure at which the monolayer has been transferred. This information indicates that the monolayer, once transferred to the mica surface, presents zones with a different tilting of the DGDG molecules that indicate a different physical state. The compression leads to a more compact fashion of the more ordered domains as it can be seen in Figure 6C at π = 33 mN·m^{-1} and in Figure 6D at π = 45 mN·m^{-1}, where practically the entire monolayer is compact, remaining only small rounded zones with the molecules in a less ordered state. On the other hand, AFM topographic images have been performed with the systems DGDG:PQ 10:1 and 20:1 (not shown) obtaining a behaviour comprised between the pure DGDG and the DGDG:PQ 5:1 (Figure 6), so only the images corresponding to π = 3 mN·m^{-1} for DGDG:PQ 10:1 and 20:1 are presented (Figure 5).

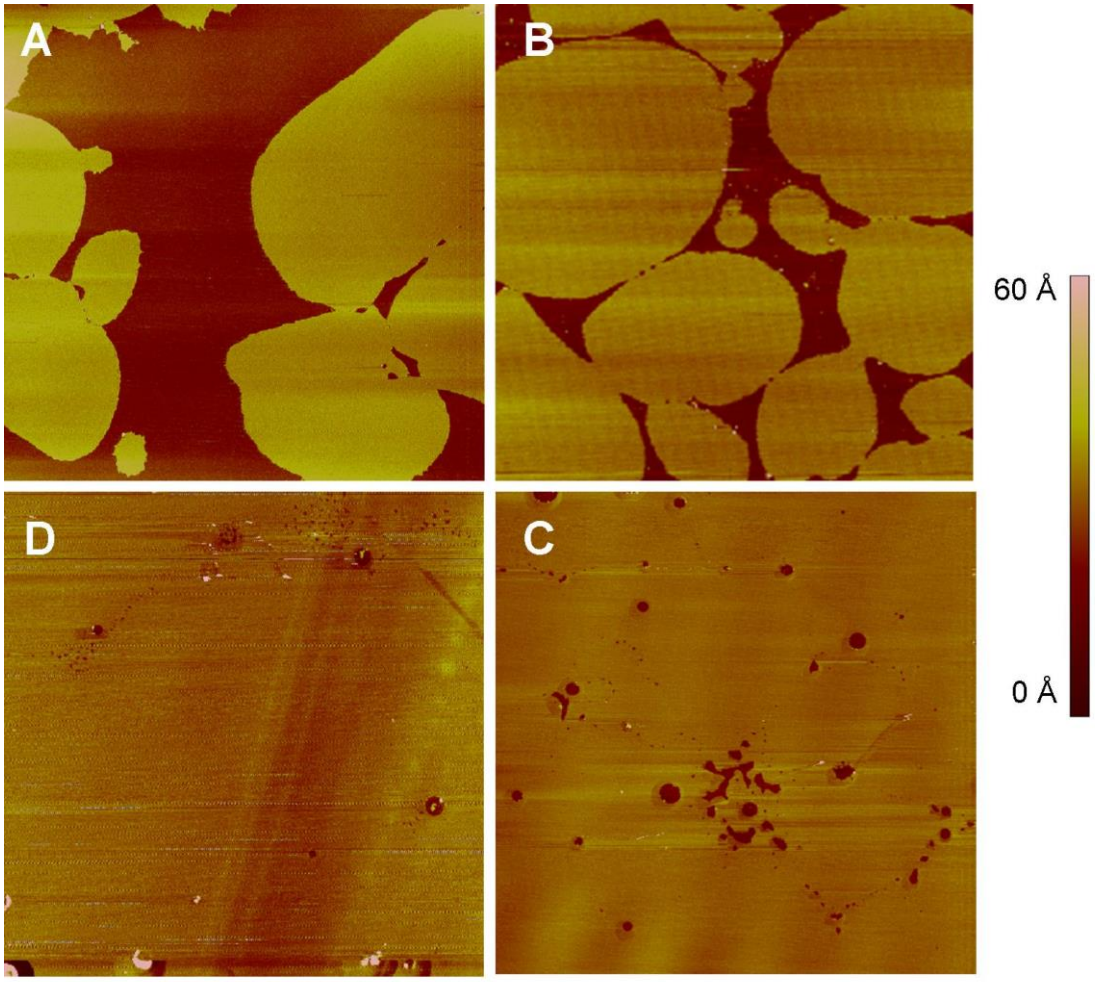

Figure 6. AFM images (10µm x 10µm) for LB films of DGDG:PQ 5:1 system transferred on mica at 21ºC at (A) π = 3 mN·m^{-1}, (B) π = 15 mN·m^{-1}, (C) π = 33 mN·m^{-1}, (D) π = 45 mN·m^{-1}.

AFM discussion

The different height observed for each tonality of both systems indicates a different tilt order of the molecules, which depends on the surface pressure and the interactions established between molecules and between the molecules with the substrate. On the other hand, it seems clear that the physical states deduced using the C_s^{-1} curves for pure DGDG are more ordered than the corresponding to DGDG:PQ at the same surface pressure, so that, the different tonalities are correlated with different ordering state, but the order that represents each tonality depends on the presence of PQ.

In order to light each physical state, we have measured the relative height between fair and dark zones of the DGDG:PQ systems, and assuming the explained height of 6 ± 2 Å for the dark brown zones referred to the mica surface, the absolute height is presented in Table II. The absolute heights obtained at each surface pressure and considering the C_s^{-1} results permit the obtaining of the physical state corresponding to each tonality for all the systems (Table III) where LC1 and LC2 have the meaning explained for pure DGDG.

Table III. Physical states of each zone (dark and fair brown) corresponding to the DGDG and DGDG:PQ systems at several surface pressures.

	DGDG		DGDG:PQ 20:1		DGDG:PQ 10:1		DGDG:PQ 5:1	
π (mN·m^{-1})	Dark	Fair	Dark	Fair	Dark	Fair	Dark	Fair
3	LE	LC1	LE	LC1	LE	LC1	LE	LC1
15	LC1	LC2	LE	LC2	LE	LC2	LE	LC1
33	LC1	LC2	LE	LC2	LE	LC2	LE	LC2

The DGDG and DGDG:PQ mixtures monolayers cover the entire mica surface at all the studied surface pressures. The non-observation of uncovered mica zones permits obtaining the proportion of each physical state. The Figure 7 presents the percentage of the monolayer in fair brown, so that, according to the Table III, the proportion of each physical state can be elucidated.

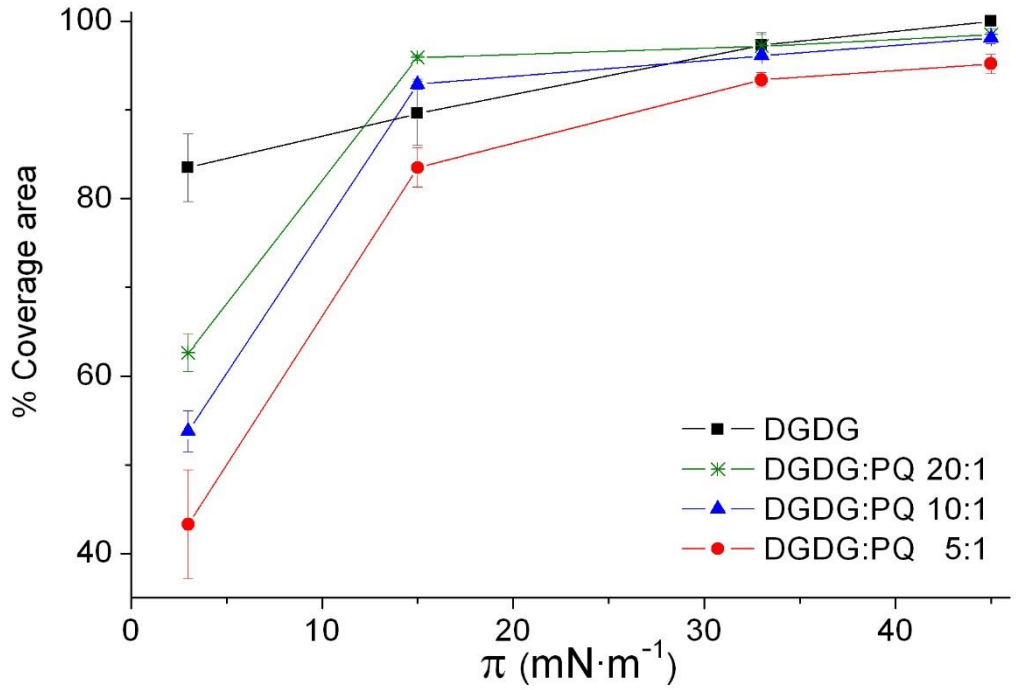

Figure 7. Monolayer coverage of the fair brown zones on the mica surface for the pure DGDG and the DGDG:PQ mixtures, calculated from AFM images.

The results obtained in Figure 7 for the DGDG:PQ systems show the expected trend of more surface covered by the compact state when decreasing the PQ content. The reason for this behaviour is that the reduced presence of PQ enhances the ordering of the DGDG molecules. Increasing the surface pressure, all the DGDG:PQ systems increases the presence of LC zones achieving at π = 15 mN·m^{-1} a nearly flat increase, which is correlated with that the major content of PQ has been rejected from the lipid matrix. On the other hand, pure DGDG presents a nearly flat increase of the area covered by the more compact phase when increasing the surface pressure. The explanation is the quick transformation of the LE or LC1 state in LC2, which leads that the entire monolayer is in a LC state at 15 mN·m^{-1}.

The simultaneous presence of two different physical states at each surface pressure for both the DGDG and DGDG:PQ systems indicates that both systems present a physical state change that implies the coexistence, from low surface pressures, of zones with low and high order of molecules (See Table III). The pure DGDG system achieves the complete LC state (Table III) at lower surface pressure than the DGDG:PQ mixtures, which is explained by the presence of PQ in the DGDG:PQ mixtures that hindrances the packing of the DGDG molecules. At the same surface pressure, the DGDG presents similar or higher ordered state for the fair zones

than the DGDG:PQ mixtures (See Table III), which indicates that part of the PQ is in the LC domains. A similar behaviour is observed for the dark zones, which also indicates the presence of PQ in the LE state. These observations indicate that PQ is present in both physical states of the DGDG:PQ mixtures and the higher affinity of the PQ for the LE state points the formation of DGDG:PQ domains (LC zones) with low PQ content and DGDG:PQ domains with high PQ content (LE zones), so establishing the LE zones as PQ rich zones. On the other hand, the LC areas correspond to DGDG zones where the low presence of PQ slightly hinders the compactness of this physical state (Figure 5).

3.3 Electrochemical behaviour

The electrochemical behaviour of the ITO-DGDG/electrolyte, ITO-PQ/electrolyte and the ITO-DGDG:PQ/electrolyte systems is studied in this section. In our experiments, three CVs are required to obtain the stationary state in the electrochemical response, presenting a good reproducibility from the third scan and at least 15 cycles.

Figure 8 presents the cyclic voltammograms at 10 $mV \cdot s^{-1}$ of the ITO-DGDG/electrolyte at π = 3 $mN \cdot m^{-1}$ and π = 33 $mN \cdot m^{-1}$, ITO-PQ/electrolyte system at π = 2 $mN \cdot m^{-1}$ and ITO-DGDG:PQ/electrolyte 5:1 transferred on ITO at several surface pressures which, in part, are the same that were selected for topographic AFM imaging on mica. In the experimental conditions, the CVs start at several positive potentials at which the PQ has the quinone ring in its oxidised form [45]. The potential is first scanned towards cathodic potentials until a final potential, which is determined by the hydrogen evolution, and then, the scan is reversed till the initial potential. Despite the fact that wider potential window has been tested, the results for pure PQ and DGDG:PQ 5:1 system at π = 3 $mN \cdot m^{-}1$ (Figure 8A) show only one redox process that we will assign as process I.

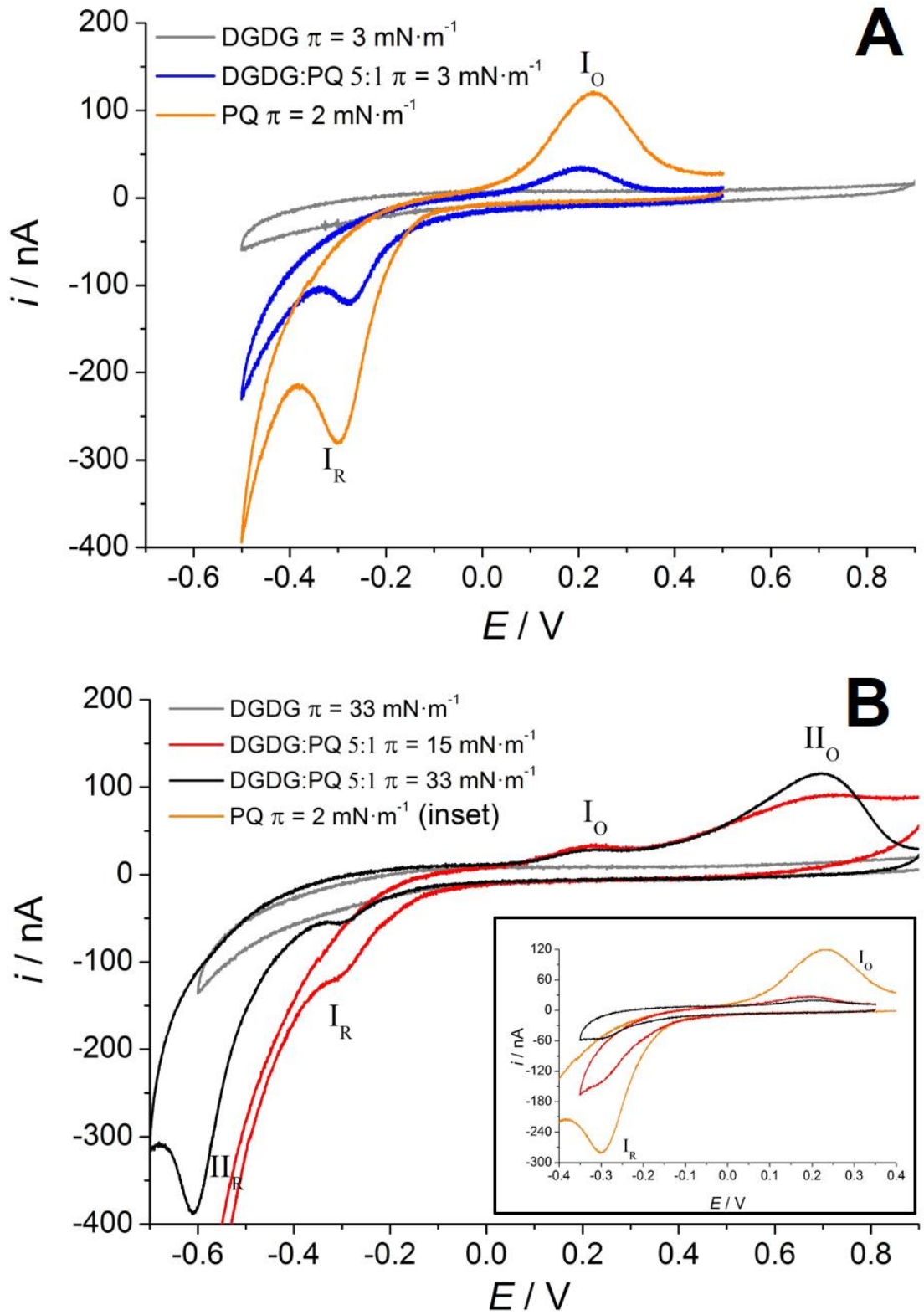

Figure 8. A and B: CVs of DGDG, PQ and DGDG:PQ 5:1 LB films transferred on ITO at the indicated surface pressures. Inset: part of the systems exposed in Figure 8A and 8B shown in shorter potential window. All CVs have been performed using 0.150 M of KCl electrochemical cell and a potassium phosphate buffered solution, at pH 7.4 and at a scan rate of 10 $mV \cdot s^{-1}$.

The DGDG:PQ 5:1 system at π = 33 $mN \cdot m^{-1}$ shows two reduction and two oxidation peaks, whereas at π = 15 $mN \cdot m^{-1}$ one reduction and two oxidation peaks are observed (Figure 8B). Comparing the potential of reduction and oxidation peaks with those in Figure 8A (see also the inset in Figure 8B), we label as process I the first redox process in Figure 8B and we assign process II to the second redox process that present the DGDG:PQ 5:1 system at this higher surface pressures. On the other hand, the ITO-DGDG:PQ/electrolyte system has also been studied with lower PQ content (not shown), presenting at all the studied surface pressures only one reduction and one oxidation peak (process I) with lower faradaic response compared with the ITO-DGDG:PQ/electrolyte 5:1 system, scanning at 10 $mV \cdot s^{-1}$. On the other hand, it is also interesting to observe that the double layer capacity of the ITO-DGDG/electrolyte experiments is fitted in the capacitive current of the ITO-DGDG:PQ/electrolyte systems (See DGDG line in Figures 8A and 8B).

In order to gain more information about the ITO-PQ/electrolyte and ITO-DGDG:PQ/electrolyte systems, voltammograms at several scan rates have been performed. Figure 9 shows the CVs of the ITO-DGDG:PQ/electrolyte 5:1 and 10:1 systems for π = 33 $mN \cdot m^{-1}$ and ITO-PQ/electrolyte system at π = 2 $mN \cdot m^{-1}$, being all experiments scanned at 200 $mV \cdot s^{-1}$. In this figure, the scan rate is increased in such way that the hydrogen evolution present in all the voltammograms at all compositions starts at more negative potentials than at 10 $mV \cdot s^{-1}$, indicating that this evolution is a quite slower process than process II. In consequence, the reduction of process I and II is unmasked and it confirms that the ITO-DGDG:PQ/electrolyte 10:1 system at π = 33 $mN \cdot m^{-1}$ also shows process II.

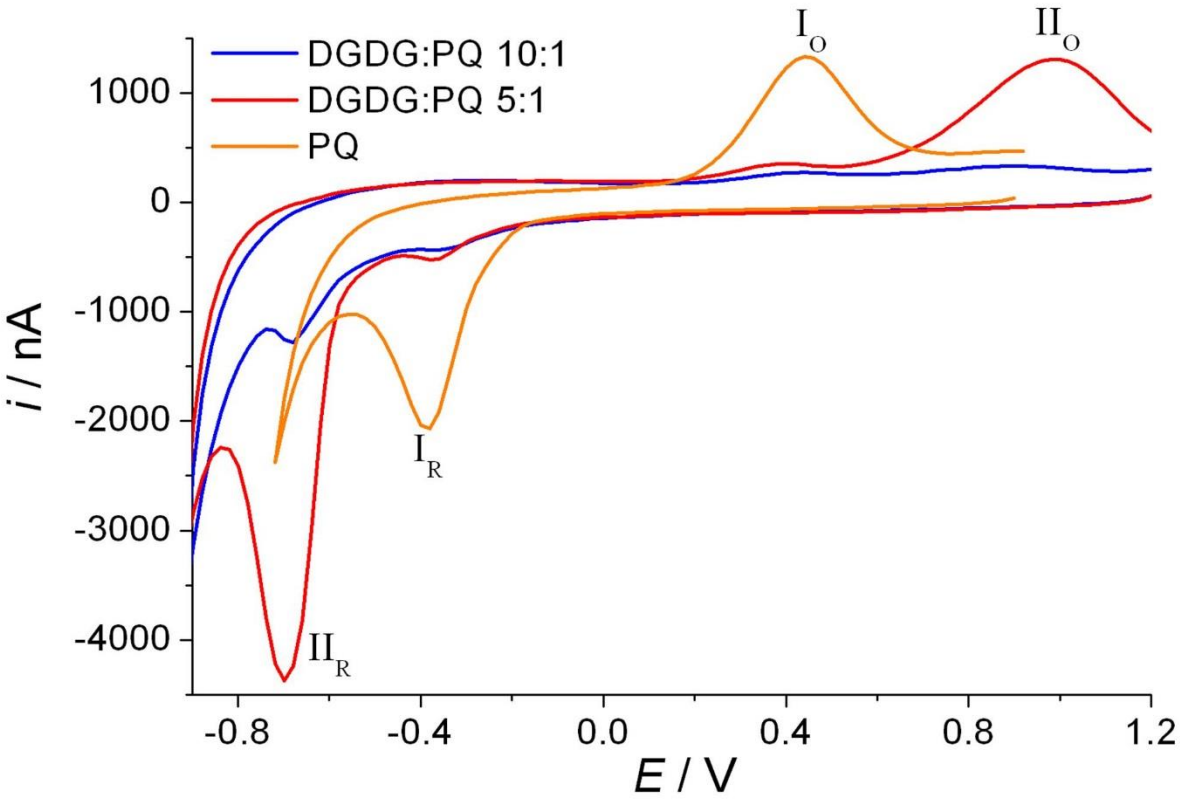

Figure 9. Cyclic voltammograms of ITO-DGDG:PQ/electrolyte 5:1 and 10:1 LB films transferred at $\pi = 33$ $mN \cdot m^{-1}$ and ITO-PQ/electrolyte system transferred at $\pi = 2$ $mN \cdot m^{-1}$, all scanned at 200 $mV \cdot s^{-1}$. All CVs have been performed using 0.150 M of KCl electrochemical cell using potassium phosphate buffered solution at pH 7.4.

Discussion of the electrochemical response of the ITO-DGDG:PQ/electrolyte system

The dependence of peak current intensity of the redox process I and II vs the scan rate has been studied for the ITO-DGDG:PQ/electrolyte 5:1 (not shown). A linear dependence has been obtained, either for the reduction and the oxidation peak currents of both process I and II. This linear dependence indicates that the PQ/PQH_2 redox couple is surface confined in both processes [46,47] and that the electron-transfer process is not diffusion controlled. Therefore, in the experimental conditions the PQ molecules have in the surface environment enough hydrogen ions to accomplish the global electron transfer reaction that at pH=7.4 is written as:

$$PQ + 2e^- + 2H^+ \rightarrow PQH_2 \qquad (7)$$

The peak shape of the voltammograms for the ITO-DGDG:PQ/electrolyte systems (Figures 8 and 9) is not symmetrical, presenting the reduction peak a sharper shape than the oxidation one. The different shape of reduction and oxidation peaks can be explained by the different hydrophilic character of the redox couple PQ/PQH_2. During the reduction scan, the larger polarity of PQH_2 compared with PQ leads the former to establish better attractive interactions by dipole-dipole or hydrogen bond between PQH_2 and DGDG headgroups [36,46]. During the oxidation scan, PQH_2 is the reactant so the possibilities of larger hydrogen bonds, increases the stabilization of the PQH_2 molecule and makes them more difficult to oxidise.

Table IV. Redox peaks potentials and the formal potential that they represent for the ITO-DGDG:PQ /electrolyte 5:1 and the ITO- PQ /electrolyte systems.

π ($mN \cdot m^{-1}$)	E_{pR} (I) (V)	E_{pO} (I) (V)	E_f (I) (V)	E_{pR} (II) (V)	E_{pO} (II) (V)	E_f (II) (V)
ITO-DGDG:PQ/electrolyte 5:1						
3	-0.28 ± 0.02	0.19 ± 0.02	-0.05 ± 0.03	-	-	-
15	-0.31 ± 0.02	0.19 ± 0.02	-0.06 ± 0.03	-	-	-
33	-0.32 ± 0.02	0.20 ± 0.02	-0.06 ± 0.03	-0.61 ± 0.02	0.70± 0.02	0.05 ± 0.03
ITO- PQ/electrolyte						
2	-0.30 ± 0.02	0.23 ± 0.02	-0.04 ± 0.03	-	-	-

In all the studied ITO-DGDG:PQ systems, the redox peaks separation for process II is larger than for process I indicating that process II is even more irreversible than process I. The formal potential of process I and II calculated as the midpoint between the reduction and oxidation peak potentials are shown in Table IV for the ITO-DGDG:PQ/electrolyte 5:1 system at π = 33 mN·m^{-1} and for the ITO-PQ/electrolyte system at π = 2 mN·m^{-1}. Table IV shows that the E_f(I) for the ITO-DGDG:PQ/electrolyte 5:1 system is close to the formal potential of the redox process I obtained for the ITO-PQ/electrolyte system, which indicates that the local environment around each PQ heads is similar in these situations [48]. Thus, for the DGDG:PQ films, we correlate the process I with the redox behaviour of PQ/PQH_2 molecules placed inside the lipid layer with direct contact or short distance between ITO and the PQ head. On the other hand, process II is more irreversible than process I, but it has more positive formal potential (close to that of benzoquinone/hydroquinone in aqueous solution $E_f \approx$ 0.14 V vs. Ag/AgCl [49]) which can be correlated with a more aqueous environment for the PQ/PQH_2 headgroups with higher H^+ ion availability nearer to the aqueous electrolyte. Therefore, we correlate process II with the redox behaviour of the PQ molecules that have been expelled from the DGDG matrix and are placed on top of the monolayer. The major irreversibility of process II compared with process I is correlated with the larger distance that the electron transfer is forced to proceed from the ITO surface to the PQ head, which induces a slowing of the overall electron-transfer rate that is often observed in SAM of electro-active molecules [48,50] and in SPB [51]. The fact that the half-width of the oxidation peak II was larger than that of I is also an indication of a different local environment of PQH_2 molecules during the oxidation process.

The charge involved in the LB monolayer transferred at each surface pressure is obtained by integrating the area under the reduction or oxidation waves. The surface coverage (Γ) is obtained from the experimental values of charge and considering the global reaction (eq. 7) for PQ in confined situation. At low surface pressures, when only process I is present in the voltammograms, the Γ_O(I) values are equal to the total surface coverage (Γ_{Otot}), but increasing the surface pressure, when process II_O appears, Γ_O(I) for the ITO-DGDG:PQ system attains a maximum value ≈ 3.5 ·10^{-12} mol·cm^{-2}. Γ_O (I) value present a slight decrease increasing the surface pressure for the DGDG:PQ 5:1 system and a continuous increase until that maximum value at lower PQ contents in the DGDG:PQ mixture.

3.4 Global sight of the DGDG:PQ system transferred on ITO using the LB technique

In this section we explain the global behaviour of the DGDG:PQ system and the position of the PQ molecules in the monolayer studying the results obtained from the used techniques. We will discuss the positions of PQ based on the explained studies for UQ (see Introduction) due to the similarities between both prenylquinones. In addition, we consider that the positions and processes that take place in the lower leaflet of a bilayer are comparable with those that take place in the LB monolayer.

The slightly lower C_s^{-1} values observed for the DGDG:PQ mixtures compared to the pure DGDG after the kink point indicate that the presence of the remaining PQ molecules (diving position, see Introduction) have little effect on the monolayers of the DGDG:PQ mixtures. The shape of the π-A isotherms, the shape of the C_s^{-1} curves and the shape of the kink point in the C_s^{-1} curves suggest that the system experiences a sudden PQ expulsion of most of the PQ content. The expulsion of the PQ from the lipid heads region leads to the diving position without ITO-PQ contact and to the swimming position, being this last position and the formation of aggregates favoured at large initial content of PQ and at ordered states, as it was previously observed [17,29,52,53]. So that, the expulsion of PQ is the way chosen by the DGDG:PQ mixture to minimize its energy at the interface [54] and to minimize the low favourable interactions between PQ and the DGDG chains. The proportion of PQ at each position (diving or swimming) is defined by the DGDG physical state and the initial PQ content.

A complete vision of the PQ positions in the DGDG:PQ monolayer can be obtained considering the thermodynamic description of the physical states, the AFM results of the DGDG:PQ 5:1 system on mica (Figure 6) and the CVs of Figures 8 and 9. Therefore, these PQ positions will be extrapolated to all the ITO-DGDG:PQ systems considering the explained presence of PQ in both physical states (LE and LC) of the DGDG:PQ mixtures. At π = 3 $mN \cdot m^{-1}$, the CVs of Figure 8 shows that only the redox process I is obtained and it presents a similar formal potential to that of process I for the ITO-PQ/electrolyte system (Table IV). The slight displacement to more negative values of the E_f(I) for the ITO-DGDG:PQ/electrolyte 5:1 system, shown in Table IV, may be related with the higher proportion of compact LC state

compared with the pure PQ or the ITO-MGDG:UQ/electrolyte 5:1 system which induces slight changes in the PQ environment that hindrance the electron transfer. Despite of these small differences, at low surface pressures, regardless the MGDG:UQ domains are in LE or LC state (Figure 6A), we correlate process I with the diving position at which the UQ is placed in the MGDG matrix and located in direct contact with the electrode surface (see the Schematic 1 at π = 3 mN·m^{-1}). The compression of the explained monolayer induces two actions: First the compactness of the LC state, so favouring the rejection of part of the PQ in diving position. On the one hand, it can be vertically rejected to the diving position without ITO-PQ contact and, on the other hand, horizontally to the remaining LE zones so enriching them in PQ. Second, the phase change from LE to LC of the remaining LE zones (Figure 6C). Further compression results in smaller but more enriched LE zones and a more compact LC state (Figure 6C and 6D). In addition it implies the rejection of the PQ molecules in diving position without ITO-PQ contact to the swimming position. In this case, the low quality of the topographic images for DGDG:PQ mixtures at π = 33 mN·m^{-1} complicate the observation of the PQ physical state but the no observation of localized higher zones suggest that the PQ are present as single molecules or small pools of molecules in LE state. In relation to this fact, we relate it to the difficulty on performing topographic images on tapping mode at high surface pressures.

The presence of enriched domains is predictable based on the Van Dijck et al. [55] observations for saturated phospholipids with the same headgroup and others studies presented in the literature [17,53,56]. In addition, Figure 6C and 6D present small LE zones in circular shape, which is the shape adopted by the monolayers to minimize the surface tension of the nascent boundary when lipid reorientate in the layer boundaries [57], and they may indicate that the composition in and out the rounded shape is different. On the other hand, the saturation of the Γ_O (I) when increasing the surface pressure at which the LB film has been transferred suggests that, when changing from LE to LC, the vertical rejection is also favoured, placing part of the PQ molecules in the swimming position in the LC zones. The gradual LE to LC physical state change permits that part of the PQ molecules get the most stable position that is the swimming position. However, the diving position can be favoured thanks to fast physical state change and/or part of the PQ molecules self-aggregate, in accordance with Roche et al. [6], forming head to head aggregates to withstand the hydrophobic environment of the lipid chain region. It is important to consider that our

experiments always presents a higher PQ content than the minimum observed in the literature for UQ aggregation (0.5-2 mol%) [17,28,58].

In order to clarify the position and organization of the DGDG and PQ molecules at each physical state, the Schematic 1 represents the position of DGDG and PQ molecules of the DGDG:PQ 5:1 system at the studied surface pressures. This Schematic 1 explains the different meaning of the fair and dark colours observed in the AFM images summarized in Table III and the PQ positions that origin the redox processes I (position I_α corresponds to diving position with ITO-PQ contact and I_β to diving position without ITO-PQ contact) and II.

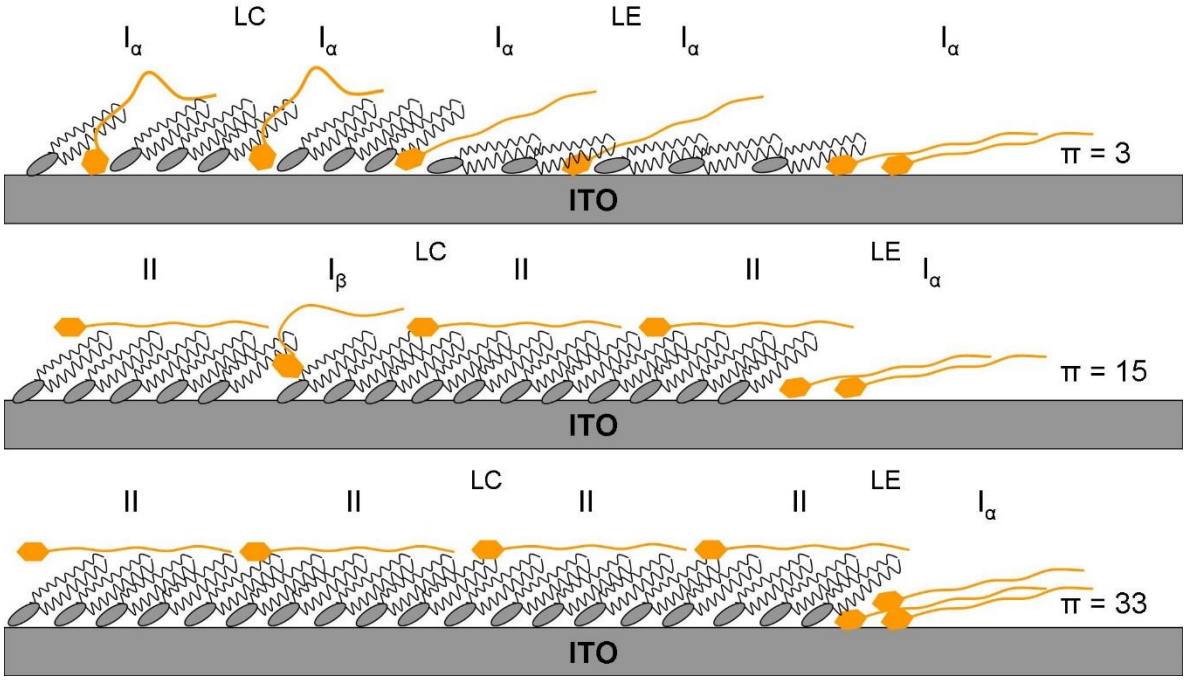

Schematic 1. Scheme of the position of DGDG and PQ molecules of the DGDG:PQ 5:1 system at several surface pressures. The labels I_α, I_β and II indicate the PQ positions that origin the redox processes I (position I_α corresponds to "diving" position with ITO-PQ contact and I_β to "diving" position without ITO-PQ contact) and II.

PQ molecules are present in two main positions in natural cell membranes being PQ_A bounded to the photosynthesis system II (PSII) and PQ_B that can free move. The electron flow from PQ_A to PQ_B is possible thanks to the higher redox potential of PQ_A due to the hydrogen bonds between the keto-oxygens and surrounding protein residues [59]. This natural behaviour can be compared with our system in which the different positions diving and swimming has also different redox potential. The redox potential for the swimming PQ is ≈

110 mV more positive than that of the diving PQ, which, by chance, is in line with the fact that the redox potential of PQ_A is ≈ 80 mV more positive than that of PQ_B [59]. The redox potential gradient permit the electron flow from the diving position to the swimming position.

The obtained results indicate that the position of PQ in the DGDG matrix can be tuned according to the surface pressure at which the LB film has been transferred, which favours the electron and proton transfer in the selected direction. The LB method permits a higher control of the PQ position compared with the vesicle fusion method observed in the literature [10, 12, 15-21]. In addition, the method performed establishes a robust lipidic matrix that is suitable to embed molecules of PQ and other molecules that can be useful in artificial photosynthesis.

4. Conclusions

The results obtained from the different used techniques and their interpretation allow us to assign the position of the PQ molecules in the lipid matrix. At low surface pressures, regardless the DGDG:PQ domains are in LE or LC state, PQ is located in diving position with the PQ placed in the DGDG matrix in direct contact with the electrode surface (I_α). The compression of the explained monolayer induces two actions: First the compactness of the LC state, so favouring the rejection of part of the PQ in diving position. On the one hand, it can be vertically rejected to the diving position without ITO-PQ contact (I_β) and, on the other hand, horizontally to the remaining LE zones so enriching them in PQ. Second, the phase change from LE to LC of the remaining LE zones. Further compression results in smaller but more enriched LE zones, a more compact LC state and it implies the rejection of the PQ molecules in diving position without ITO-PQ contact to the swimming position. The proportion of PQ at each position (diving or swimming) is defined by the lipid physical state and the initial PQ content. On the other hand, the LB method permits a higher control of the PQ position compared with the vesicle preparation method.

The position of PQ in the DGDG matrix can be tuned according to the surface pressure at which the LB film has been transferred, which favours the electron and proton transfer in the desired direction.

Acknowledgements

The authors thank the economic support of the Spanish Government, through the project CTQ2007-68101-C02, and of the Catalonia Autonomic Government, through the project SGR2009-277. J Hoyo thanks to Universitat Politècnica de Catalunya its PhD grant.

5. References

[1] H.Gao, G. Luo, J. Feng, A.L. Ottova, H. Ti Tien, Photoelectric conversion properties of bilayer lipid membranes self-assembled on an ITO substrate. J. Electroanal. Chem. 496 (2001) 158–161.

[2] D. Berti, G. Caminatia, P. Baglioni, Functional liposomes and supported lipid bilayers: towards the complexity of biological archetypes. Phys. Chem. Chem. Phys. 13 (2011) 8769–8782.

[3] C. Ge, K.S. Orosz, N.R. Armstrong, S.S. Saavedra, Poly(aniline) nanowires in sol-gel coated ITO: a pH-responsive substrate for planar supported lipid bilayers. ACS Appl Mater Interfaces. 7 (2011) 2677-2685.

[4] W. Zhan, K. Jiang, A Modular Photocurrent Generation System Based on Phospholipid Assembled Fullerenes. Langmuir 24 (2008) 13258-13261.

[5] A. Iglic, Advances in Planar Lipid Bilayers and Liposomes; Ed. Elsevier, San Diego, California. Vol 13, 2011.

[6] N. Mizusawa, H. Wada, The role of lipids in photosystem II. Biochim Biophys Acta. 1817 (2012) 194-208.

[7] C. Glöckner, The donor and acceptor side of photosystem II: Structural and functional investigations. Ph.D. thesis, Technischen Universität Berlin, Berlin, 2013.

[8] P. Dörmann, G. Hölzl, Wada, Hajime; Murata, Norio (Eds.) Essential and Regulatory Functions, The Role of Glycolipids in Photosynthesis. Springer, Dordrecht, The Netherlands, 2010, 265-282.

[9] A.G. Ivanov, L. Hendrickson, M. Krol, E. Selstam, G. Oquist, V. Hurry, N.P. Huner, Digalactosyldiacylglycerol deficiency impairs the capacity for photosynthetic inter-system electron transport and state transitions in Arabidopsis thaliana due to photosystem I acceptor-side limitations. Plant Cell Physiol. 47 (2006) 1146-1157.

[10] G. Lenaz, B. Samori, R. Fato, M. Battino, G. Parenti Castelli, I. Domini, Localization and preferred orientations of ubiquinone homologs in model bilayers, Biochem. Cell. Biol. 70 (1992) 504–514.

[11] J. A. Söderhäll, A. Laaksonen, Molecular Dynamics Simulations of Ubiquinone inside a Lipid Bilayer. J. Phys. Chem. B, 105 (2001) 9308-9315.

[12] F.J. Aranda, J.C. Gomez-Fernandez, The interaction of ubiquinone-10 and ubiqui-nol-10 with phospholipid bilayers. A study using differential scanning calorimetry and turbidity measurements, Biochim. Biophys. Acta 820 (1985) 19–26.

[13] J. Kruk, B. Myśliwa-Kurdziel, M. Jemioła-Rzeminiska, K. Strzałka, Fluorescence lifetimes study of alpha-tocopherol and biological prenylquinols in organic solvents and model membranes. Photochem. Photobiol. 82 (2006) 1309-1314.

[14] R. M. Venable, Y. Zhang, B. J. Hardy, R. W. Pastor, Molecular dynamics simulations of a lipid bilayer and of hexadecane. An investigation of membrane fluidity. Science 262 (1993) 223–226.

[15] H. Katsikas, P.J. Quinn, Fluorescence probe studies of the distribution of ubiquinone homologues in bilayers of dipalmitoylglycerophosphocholine, Eur. J. Biochem. 131 (1983) 607– 612.

[16] M. Ondarroa, P.J. Quinn, A difference infrared-spectroscopic study of the interaction of ubiquinone-10 with phospholipid bilayers, Biochem. J. 240 (1986) 325– 331.

[17] M. Jemiola-Rzeminska, J. Kruk, M. Skowronek, K. Strzalka, Location of ubiquinone homologues in liposome membranes studied by fluorescence anisotropy of diphenyl-hexatriene and trimethylammonium-diphenyl-hexatriene. Chem. Phys. Lipids. 79 (1996) 55-63.

[18] J. Hoyo, E. Guaus, J. Torrent-Burgues, F. Sanz, Electrochemical behaviour of mixed LB films of ubiquinone – DPPC. J. Electroanal. Chem. 669 (2012) 6-13.

[19] R. Fato, M. Battino, M. Degli Esposti, G. Parenti Castelli, G. Lenaz, Determination of partition and lateral diffusion coefficients of ubiquinones by fluorescence quenching of n-(9-anthroyloxy)stearic acids in phospholipid vesicles and mitochondrial membranes. Biochemistry 25 (1986) 3378-3390.

[20] D. Marchal, W. Boireau, J.M. Laval, J. Moiroux, C. Bourdillon, Electrochemical measurement of lateral diffusion coefficients of ubiquinones and plastoquinones of various isoprenoid chain lengths incorporated in model bilayers. Biophys. J. 74 (1998) 1937-1948.

[21] H. Katsikas, P.J. Quinn, The polyisoprenoid chain length influences the interaction of ubiquinones with phospholipid bilayers, Biochim. Biophys. Acta 689 (1982) 363–369.

[22] J. Hoyo, E. Guaus, G. Oncins, J. Torrent-Burgués, F. Sanz, Incorporation of Ubiquinone in Supported Lipid Bilayers on ITO. J. Phys. Chem. B, 117 (2013) 7498–7506

[23] G. Cevc, D. Marsh, Phospholipid Bilayers. Physical Principles and Models. Wiley-Inrscience, New York, 1987.

[24] S. Morandat, K. El Kirat, Cytochrome c provokes the weakening of zwitterionic membranes as measured by force spectroscopy. Colloids Surf. B 82 (2011) 111−117.

[25] A. Bruno, C. Rossi, G. Marcolongo, A. Di Lena, A. Venzo, C.P. Berrie, D. Corda, Selective in vivo anti-inflammatory action of the galactolipid monogalactosyldiacylglycerol. Eur. J. Pharmacol. 524 (2005) 159-168.

[26] J.Hoyo, E. Guaus, J. Torrent-Burgues, Biomimetic monolayer films of monogalactosyldiacylglycerol incorporating ubiquinone. J. Colloid Interface Sci. 384 (2012) 189−197.

[27] J. Kruk, K. Strzałka, R.M. Leblanc, Monolayer study of plastoquinones, alpha-tocopherol quinone, their hydroquinone forms and their interaction with monogalacto-syldiacylglycerol. Charge-transfer complexes in a mixed monolayer. Biochim. Biophys. Acta 1112 (1992) 19-26.

[28] R. Bilewicz, M. Majda, Monomolecular Langmuir-Blodgett films at electrodes. Formation of passivating monolayers and incorporation of electroactive reagents. Langmuir 7 (1991) 2794–2802.

[29] M. Jemioła-Rzemińska, B. Myśliwa-Kurdziel, K. Strzałka, The influence of structure and redox state of prenylquinones on thermotropic phase behaviour of phospholipids in model membranes. Chem Phys Lipids 114 (2002) 169-180.

[30] P. Vitovič, D.P. Nikolelis, T. Hianik, Study of calix [4] resorcinarene–dopamine complexation in mixed phospholipid monolayers formed at the air|water interface. Biochim. Biophys. Acta 1758 (2006) 1852-1861.

[31] A. Es-Sounni, R.M. Leblanc, Mixed monolayer studies of chlorophyll a and plastoquinone 9 at the nitrogen-water interface. Langmuir 8 (1992) 1578–1581.

[32] B. Gzyl-Malcher, M. Filek, K. Makyła, M. Paluch, Differences in surface behaviour of galactolipids originating from different kind of wheat tissue cultivated in vitro. Chem Phys Lipids 155 (2008) 24-30.

[33] L. Zhao, S-S. Feng, Effects of lipid chain length on molecular interactions between paclitaxel and phospholipid within model biomembranes. J. Colloid and Interface Sci. 274 (2004) 55–68.

[34] J. Sanchez, A. Badia, Atomic force microscopy studies of lateral phase separation in mixed monolayers of dipalmitoylphosphatidylcholine and dilauroylphosphatidylcholine. Thin Solid Films 440 (2003) 223–239.

[35] Y. Roche, P. Peretti, S. Bernard, Influence of the chain length of ubiquinones on their interaction with DPPC in mixed monolayers. Biochim Biophys Acta. 1758 (2006) 468-478.

[36] J. Kruk, K. Strzałka, R.M. Leblanc, Monolayer study of plastoquinones, alpha-tocopherol quinone, their hydroquinone forms and their interaction with monogalactosyldiacylglycerol. Charge-transfer complexes in a mixed monolayer. Biochim. Biophys. Acta 1112 (1992) 19-26.

[37] S. Baoukina, L. Monticelli, H.J. Risselada, S.J. Marrink, D.P. Tieleman, The molecular mechanism of lipid monolayer collapse. Proc. Natl. Acad. Sci. U S A. 105 (2008) 10803–10808.

[38] R.A. Ridsdale, N. Palaniyar, F. Possmayer, G. Harauz, Formation of folds and vesicles by dipalmitoylphosphatidylcholine monolayers spread in excess. J. Membr. Biol. 180 (2001) 21-32.

[39] J. Ding, I. Doudevski, H.E. Warriner, T. Alig, J.A. Zasadzinski, Nanostructure Changes in Lung Surfactant Monolayers Induced by Interactions between Palmitoyloleoyl-phosphatidylglycerol and Surfactant Protein B. Langmuir 19 (2003) 1539–1550.

[40] T.F. Alig, H.E. Warriner, L. Lee, J.A. Zasadzinski, Electrostatic Barrier to Recovery of Dipalmitoylphosphatidylglycerol Monolayers after Collapse. Biophys J. 86 (2004) 897–904.

[41] C. Bottier, J. Géan, F. Artzner, B. Desbat, M. Pézolet, A. Renault, D. Marion, V. Vié, Galactosyl headgroup interactions control the molecular packing of wheat lipids in Langmuir films and in hydrated liquid-crystalline mesophases. Biochim Biophys Acta 1768 (2007) 1526-1540.

[42] B.S. Chu, A.P. Gunning, G.T. Rich, M.J. Ridout, R.M. Faulks, M.S. Wickham, V.J. Morris, P.J. Wilde, Adsorption of bile salts and pancreatic colipase and lipase onto digalactosyldiacylglycerol and dipalmitoylphosphatidylcholine monolayers. Langmuir 26 (2010) 9782-9793.

[43] P. Toimil, G. Prieto, J. Jr. Miñones, F. Sarmiento, A comparative study of F-DPPC/DPPC mixed monolayers. Influence of subphase temperature on F-DPPC and DPPC monolayers. Phys. Chem. Chem. Phys. 12 (2010) 13323-13332.

[44] H. Yun, Y-W. Choi, N.J. Kim, D. Sohn, Physicochemical Properties of Phosphatidylcholine (PC) Monolayers with Different Alkyl Chains, at the Air/Water Interface. Bull. Korean Chem. Soc. 24 (2003) 377-383.

[45] P.J. Quinn, M.A. Esfahani, Ubiquinones have surface-active properties suited to transport electrons and protons across membranes. Biochem. J. 185 (1980) 715–722.

[46] L. Becucci, F. Scaletti, R. Guidelli, Gel-phase microdomains and lipid rafts in monolayers affect the redox properties of ubiquinone-10. Biophys J. 101 (2011) 134-143.

[47] A.J. Bard, L.R. Faulkner, Electrochemical Methods. Fundamentals and Applications, John Wiley & Sons, New York, 2001.

[48] H. G. Hong, W. Park, Electrochemical characteristics of hydroquinone-terminated self-assembled monolayers on gold. Langmuir 17 (2001) 2485–2492.

[49] Park, H.; Park, J-S.; Shim; Y-B. Redox reaction of benzoquinone on a lipid coated glassy carbon electrode. J. Electroanal. Chem. 1997, 438, 113-119.

[50] Ma, W.; Li, D-W.; Sutherland, T.C.; Li, Y.; Long, Y-T; Chen, H-Y. Reversible Redox of NADH and NAD+ at a Hybrid Lipid Bilayer Membrane Using Ubiquinone. J. Am. Chem. Soc. 2011, 133, 12366–12369.

[51] Gao, H.; Luo, G.A.; Feng, J.; Ottova, A.L.; Tien, H.T. Fabrication and photoelectric properties of self-assembled bilayer lipid membranes on conducting glass. J Photochem Photobiol B. 2000, 59, 87-91.

[52] R. Bilewicz, Voltammetric Probing of Multicomponent Langmuir - Blodgett Monolayers Part I - Monolayers Containing Ubiquinone (Q10). Pol. J. Chem. 67 (1993) 1695-1704.

[53] A. Ausili, A. Torrecillas, F. Aranda, A.D. Godos, S. Sánchez-Bautista, S. Corbalán-García, J.C. Gómez-Fernández, Redox state of coenzyme Q10 determines its membrane localization, J. Phys. Chem. B 112 (2008) 12696–12702.

[54] D. Guay, R. M. Leblanc, Excess free energies of interaction of chlorophyll a with α-tocophelquinone and plastoquinone 3 and 9. A mixed-monolayer study. Langmuir 3 (1987) 575–580.

[55] P.W. Van Dijck, A.J. Kaper, H.A. Oonk, J. de Gier, Miscibility properties of binary phosphatidylcholine mixtures. A calorimetric study. Biochim Biophys Acta. 470 (1977) 58-69.

[56] E.L. Ulrich, M.E. Girvin, W.A. Cramer, J.L. Markley, Location and Mobility of Ubiquinones of Different Chain Length in Artificial Membrane Vesicles. Biochemistry 24 (1985) 2501-2508.

[57] Z.V. Leonenko, A. Carnini, D.T. Cramb, Supported planar bilayer formation by vesicle fusion: the interaction of phospholipid vesicles with surfaces and the effect of gramicidin on bilayer properties using atomic force microscopy. Biochim. Biophys. Acta 1509 (2000) 131-147.

[58] M.R. Moncelli, L. Becucci, A. Nelson, R. Guidelli, Electrochemical modeling of electron and proton transfer to ubiquinone-10 in a self-assembled phospholipid monolayer. Biophys J. 70 (1996) 2716-2726.
[59] Glöckner, C. The donor and acceptor side of photosystem II: Structural and functional investigations. Ph.D. Thesis, Technische Universität Berlin, Berlin, 2013.